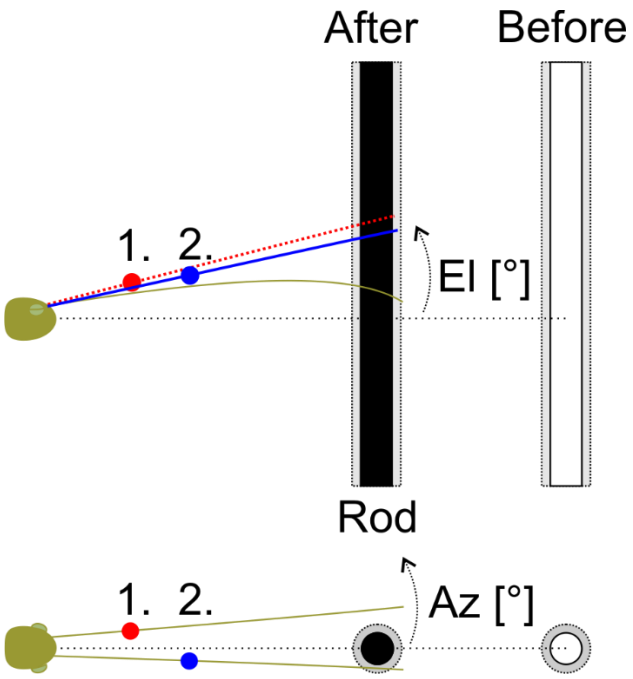

Fig. S1. Antennal contact estimation. Top and bottom panels show schematic side and top views of the experimental situation, respectively. All sizes and distances are drawn to scale. For simplicity, the vertical rod is shown at the central stimulus position (azimuth 0°), before (shaded) and after (solid) being moved into the antennal working-range. Elevation (El [°]) and azimuth (Az [°]) angles are indicated in side and top view, respectively. For motion capture of antennal movement, retro-reflective markers were placed on the proximal third of either flagellum, with the left marker (red) always being placed more proximally than the right marker (blue). Different distances improved tracking reliability but introduced an asymmetry in the estimate of the antennal elevation angles. Dotted red and solid blue lines in the side view show the linear approximation of the left and right antenna, respectively. The linear approximation neglects the slight downward curvature of the distal flagellum. Assuming the same elevation angle for both antennae, a systematic offset in the estimated elevation angle occurred, being larger for the left antenna. Accordingly, estimated antennal contact locations have a systematic upward bias. Note that this vertical bias did not affect the contact detection with the vertical rod. Antennal contacts were detected whenever the antennal azimuth was in the range filled by the rod plus a circular threshold environment (grey zones in schematic). Since markers were always placed on the dorsal surface of the flagellum, the azimuth estimates of the antennae were not biased.

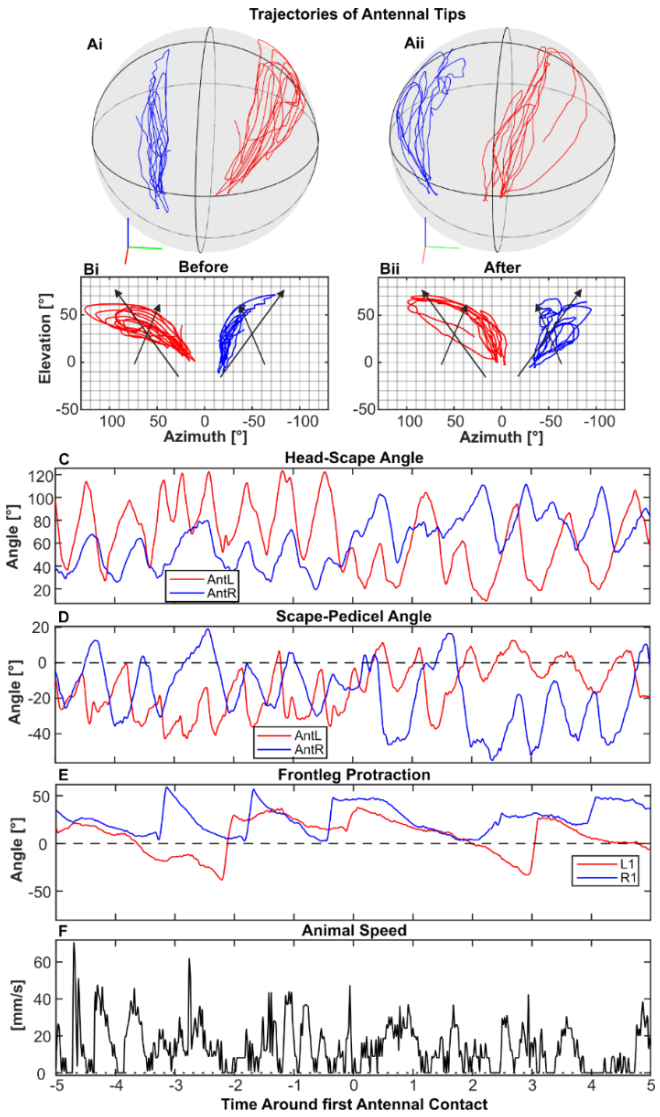

Fig. S2. Antennal movement analysis and additional measurements not used in this study. Same trial as in Fig. 2. A) Tip trajectories of the left (red) and right (blue) antenna, projected on a sphere, 5 s before (Ai) and after (Aii) the first contact event (time 0 in time courses). B) Corresponding azimuth and elevation projection of left (red) and right (blue) antennal pointing direction for the same 5 s episodes as for the spherical trajectories above. Note that the histograms in Fig. 6 and Suppl. Fig. S4 were calculated from single trial data like this. The black arrows illustrate the approximate movement directions of the antennal head-scape (arrows pointing dorso-laterally) and scape-pedicel joints (arrows pointing dorso-medially). C, D) Given the known joint axis orientations of *C. morosus,* both the head-scape joint angles (C) and the scape-pedicel joint angles (D) can be calculated by inverse kinematics (Krause and Dürr, 2004). Note how after the first antennal contact event (time > 0 s) the scape-pedicel time courses of the left (red) and right antenna shift to lower and higher values, respectively (C), corresponding to a ventro-medial shift of the left (red) and a dorso-lateral shift of the right (blue) trajectories between Bi and Bii. Similarly, the relative upward and downward shifts of the left (red) and right (blue) scape-pedicel joint angles in D correspond to dorso-medial and ventro-lateral shifts of the left (red) and right (blue) antennal trajectories, respectively (Bi and Bii). E, F) Further measured variables that were not used in the present paper include the protraction/retraction movements of the left (L1, red) and right (R1, blue) front legs (E), and the translational speed of the animal (F).

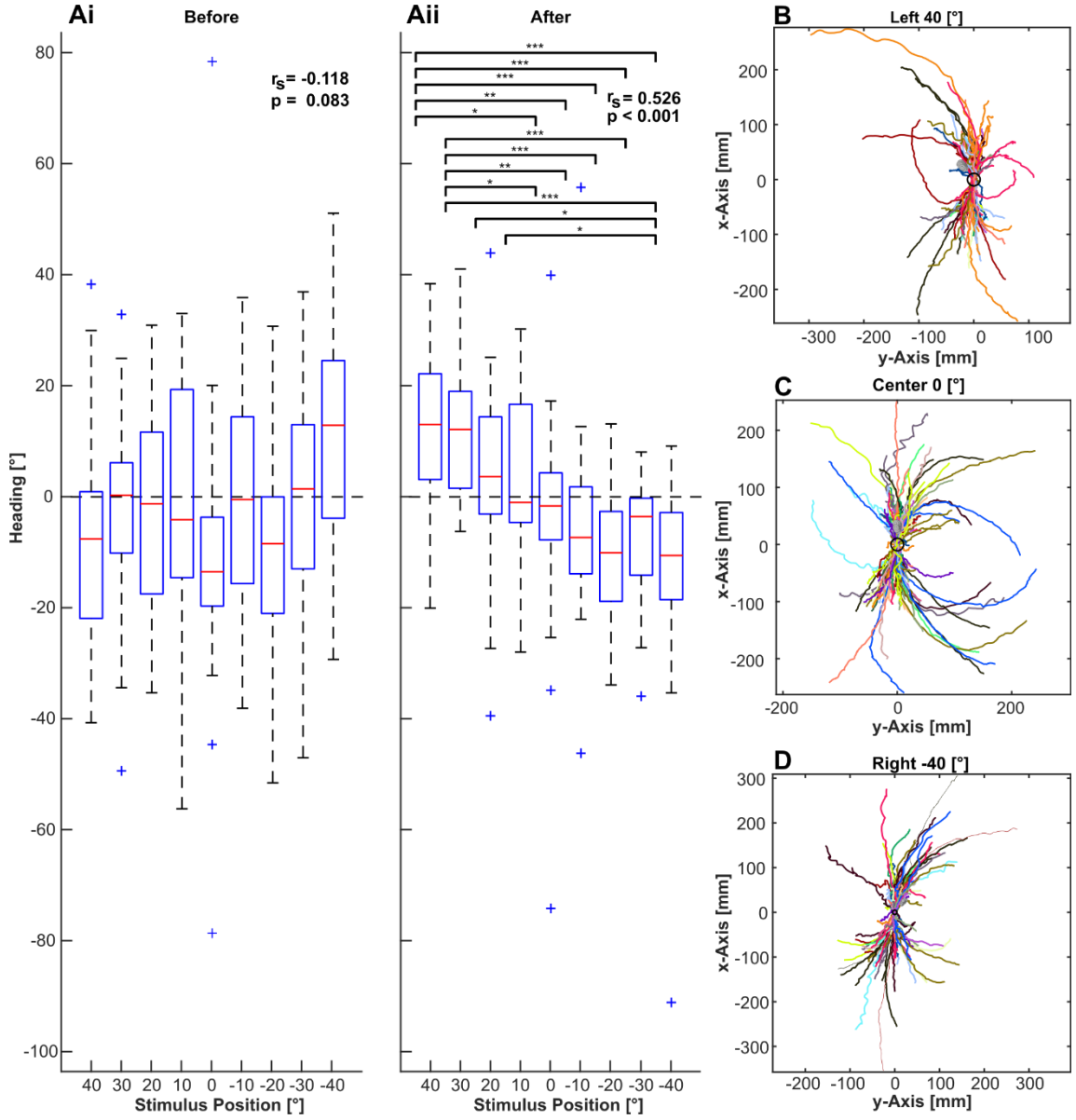

Fig. S3. Animals turn towards the tactile stimulus. Same analysis and graph details as in Fig. 5 but for the entire dataset, i.e., including trials in which the animals grasped the rod with a front leg. The overall similarity with Fig. 5 indicates that the exclusion of leg-contact trials does not affect any conclusion made. (Ai and Aii) Mean heading during walking episodes before (Ai) and after (Aii) first antennal contact with the rod. Box plots show distributions of per-animal means. Numbers of animals and trials in Table 1 B. r_S and p values correspond to a Spearman rank correlation. Pair-wise significance levels show results of a post-hoc analysis following a Kruskal-Wallis test (* p <0.05; ** p < 0.01; *** p<0.001). B-D) Animal walking trajectories, shown for all trials of the stimulus conditions -40 °, 0 ° and 40 °. Different colors indicate different animals. Trajectories were centered on the position where the first antennal contact with the rod occurred (black circle) and rotated such that their heading was 0 degrees at this position. Hence the lower and upper parts of the plots show the trajectories before and after fist antennal contact, respectively.

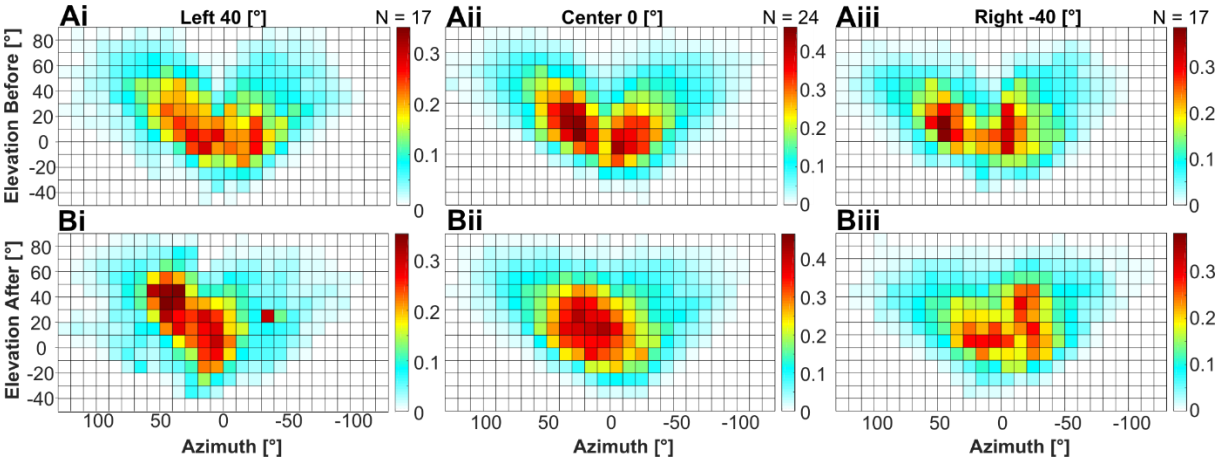

Fig. S4. Active exploration range of the antennae shifts towards stimulus location. Other than Fig. 6, these color-coded maps show antennal azimuth and elevation relative to the prothorax, thus including head movement. A, (top row): before and B (bottom row) after first antennal contact with the rod. Data are averages of normalized per-animal histograms. N gives the number of animals.

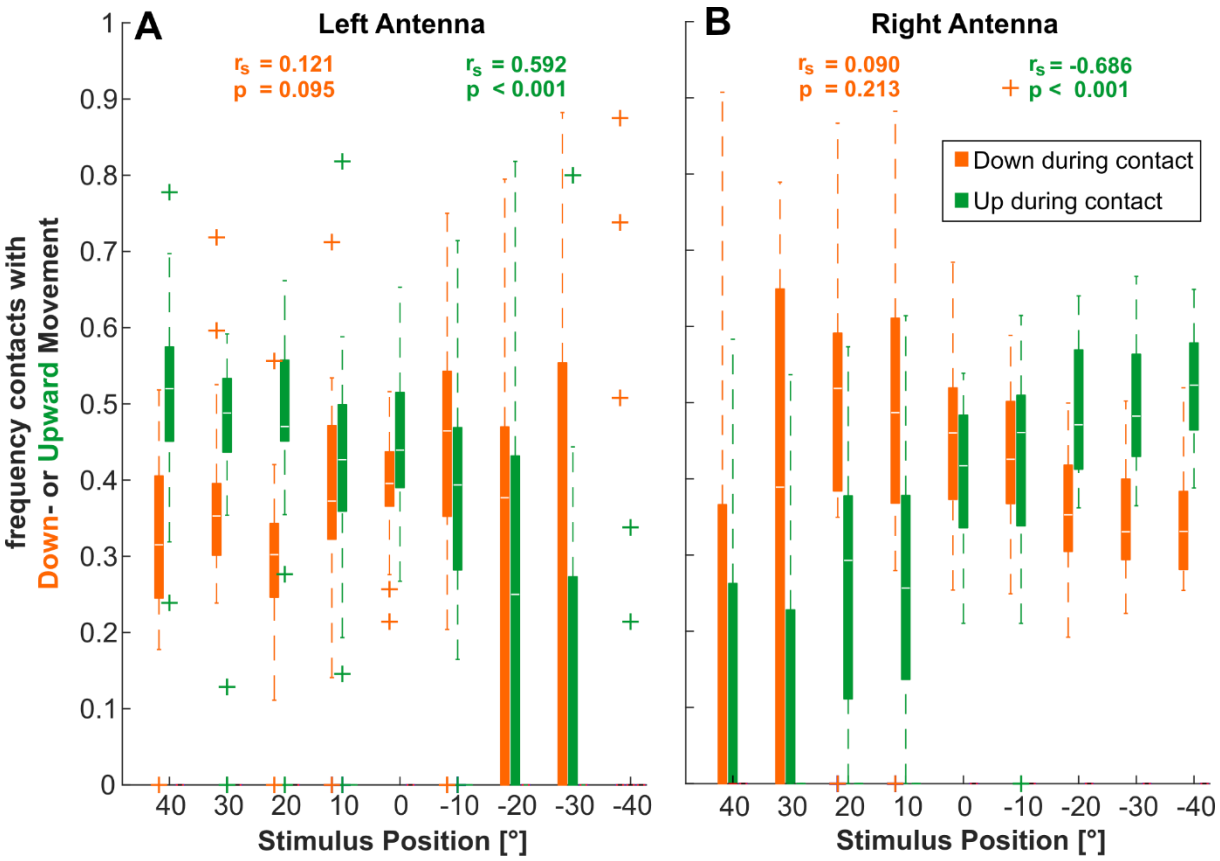

Fig. S5. Antennal movement during contact depends on stimulus position. Boxplots show the relative frequency of downward- (orange) and upward (green) movement during contact events. Relative frequency of upward movement increases with increasingly ipsilateral contact locations, whereas that of downwards movement is highest for contralateral contact locations. r_S and p values correspond to Spearman's rank correlation. For numbers of animals and trials see Table 1 (B).

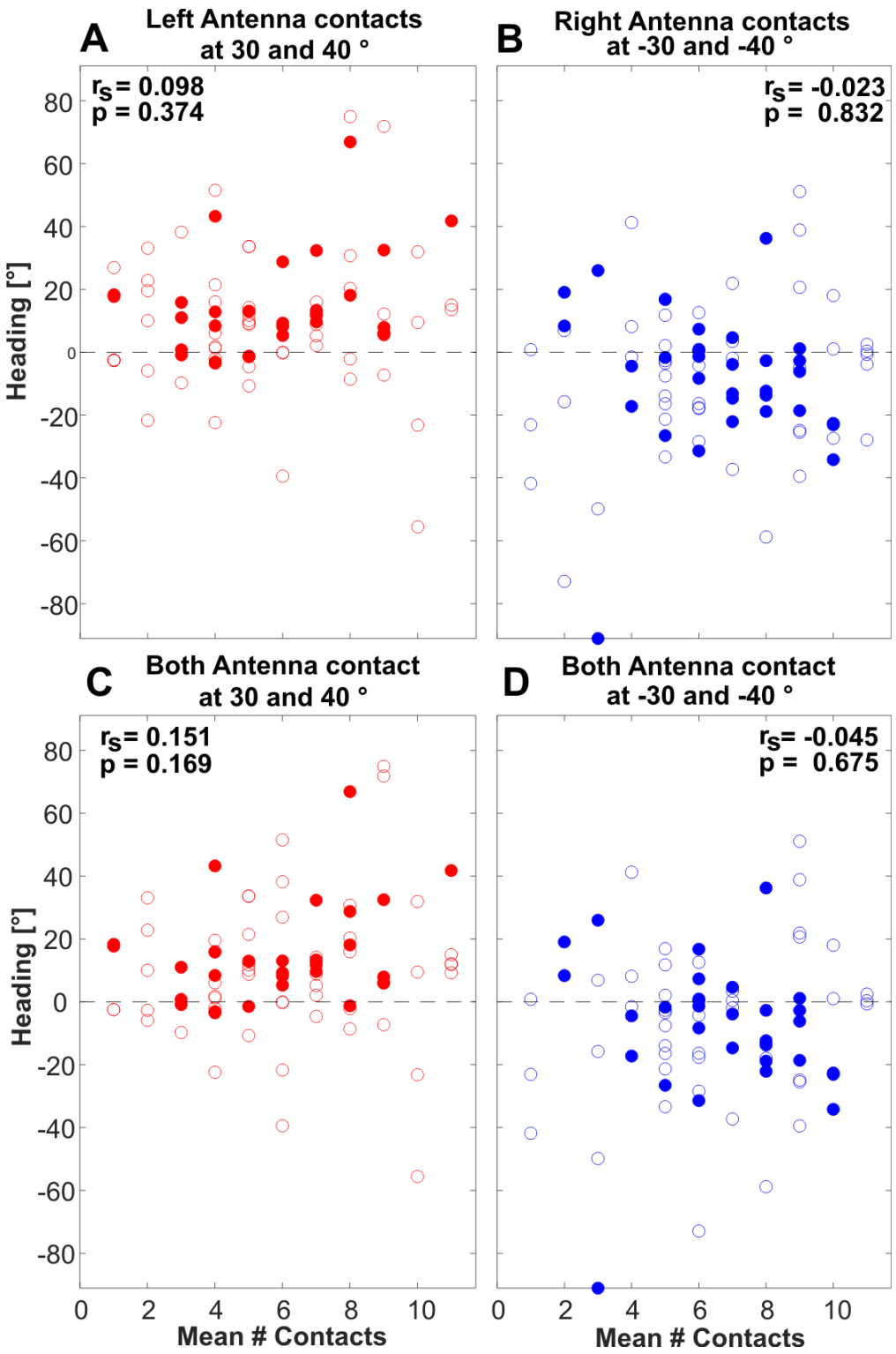

Fig. S6. Change in heading does not correlate with number of antennal contacts per trial. Change in heading is plotted against number of antennal contacts per trial. Only trials with stimulus positions ±30° or ±40° were included, as change of heading was strongest for these stimulus positions. (A, B) Only contacts of the ipsilateral antenna were included, i.e. (A) contacts of the left antenna stimulus positions 30°(red open circles) and 40° (red filled circles), and (B) contacts of the right antenna stimulus positions -30° (blue open circles) and -40° (blue filled circles). (C, D) Same analysis as above, but including rare contact events of the respective contralateral antenna. None of the panels show a significant correlation between number of antennal contacts and change in heading. r_S and p values correspond to Spearman's rank correlation. For numbers of animals and trials see Table 1 (B).